Available online at www.sciencedirect.com
SCIENCE DIRECT®
Thermochimica Acta 425 (2005) 75–89
thermochimica acta
www.elsevier.com/locate/tca

Structure and thermal behavior of nanocrystalline boehmite

Pierre Alphonse*, Matthieu Courty

CIRIMAT, UMR-CNRS 5085, Université Paul Sabatier, 118 route de Narbonne, 31062 Toulouse Cedex 04, France

Received 8 March 2004; received in revised form 11 June 2004; accepted 21 June 2004
Available online 2 September 2004

Abstract

First, the structural features of nanocrystalline boehmite synthesized by hydrolysis of aluminum sec-butoxide according to the Yoldas method are reported. The nanosized boehmite consists of rectangular platelets averaging 8 by 9 nm and 2–3 nm in thickness which contain a large excess of water. Dehydration by heating under vacuum induced an increase in the specific surface area, down to a minimum water content (~0.2 H_2O per Al_2O_3); values up to 470 m^2/g can be reached. However this enlargement of specific surface area only results from water loss, the surface area remaining constant. The particle morphology, the excess of water, as well as the specific surface area, depend on the amount of acid used for the peptization during the synthesis. Second, a comprehensive investigation of the dehydration kinetics is presented. The simulations of the non-isothermal experiments at constant heating rates show that thermally stimulated transformation of nanocrystalline boehmite into alumina can be accurately modeled by a 4-reaction mechanism involving: (I) the loss of physisorbed water, (II) the loss of chemisorbed water, (III) the conversion of boehmite into transition alumina, (IV) the dehydration of transition alumina (loss of residual hydroxyl groups). The activation energy of each step is found to be very similar for experiments done in various conditions (heating rate, atmosphere, kind of sample,. . .).

Keywords: Boehmite; Transition alumina; Non-isothermal kinetics; Computer simulation

1. Introduction

Alumina is a low cost material used in many domains like catalysis, ceramics and mechanical ceramics, refractory, electrotechnology, electronics, bio-medical,. . .. The wide variety of these applications comes from the fact that alumina occurs in two forms, corundum or α-alumina with an hexagonal close-packing of oxygen ions and transition aluminas with a cubic close packing of oxygen. Transition aluminas include a series of metastable forms that exist on an extended temperature range, but all of them lead to α-alumina by calcining at high temperatures. Corundum has excellent mechanical, electrical, thermal, and optical properties. Transition aluminas are widely used as adsorbents, catalysts, catalyst supports, and membranes because of their high surface area, mesoporosity, and surface acidity.

Transition aluminas are prepared by calcining aluminum hydroxides. Starting from different hydroxides leads to different forms having different thermal stability, surface acidity and textural properties. Among aluminum hydroxides, boehmite, aluminum oxyhydroxide (AlOOH) is an important precursor because the heat treatment of boehmite produces a series of transition aluminas from γ-Al_2O_3 and η-Al_2O_3 to δ-Al_2O_3, and θ-Al_2O_3, which exhibit high surface areas (200–500 m^2/g) and thermal stability up to 1000 °C.

The structures of the transition aluminas all are based on a face-centered cubic (fcc) array of oxygen anions. The structural differences between these forms only involve the arrangement of aluminum cations in the interstices of the fcc array of oxygen anions. γ-Al_2O_3 and η-Al_2O_3 have defect spinel structures [1]. δ-Al_2O_3 has a tetragonal superstructure of the spinel lattice with one unit-cell parameter tripled [1] and θ-Al_2O_3 has a monoclinic structure [2]. η-Al_2O_3 is

* Corresponding author. Tel.: +33 5 61 55 62 85; fax: +33 5 61 55 61 63.
E-mail addresses: alphonse@chimie.ups-tlse.fr (P. Alphonse), courty@chimie.ups-tlse.fr (M. Courty).

0040-6031/$ – see front matter © 2004 Elsevier B.V. All rights reserved.
doi:10.1016/j.tca.2004.06.009

produced by dehydration of bayerite $Al(OH)_3$, whereas γ-Al_2O_3 is formed by dehydration of boehmite. Upon heating, γ-Al_2O_3 and η-Al_2O_3 are gradually converted in θ-Al_2O_3. In the case of γ-Al_2O_3, this transformation occurs via the formation of δ-Al_2O_3 which is not observed for η-Al_2O_3.

Boehmite was thought to exist under two distinct forms, well-crystallized boehmite and pseudoboehmite (also called gelatinous boehmite) [3,4], with significantly different morphologies, porosity, and surface areas. However, recent crystallographic studies [5–9] have clearly demonstrated that pseudoboehmite is simply micro- or rather nano-crystallized boehmite, the differences observed between the two forms coming from the difference in crystallite size.

Since the oxygen sublattice of boehmite is cubic packing, boehmite dehydration to form transition aluminas and the further transformations through the transition alumina series only involve short-range rearrangements of atoms in the crystal structure. These conversions are topotactic and require only a small energy. Hence, the temperatures at which they are observed are variable and depend on the crystallinity of the boehmite precursor as well as on the thermal treatment conditions. Therefore, the characteristics of the transition aluminas, such as specific area, porosity, pore-size distribution, acidity, are deeply affected by the microscopic morphology of the boehmite precursor.

The identification and characterization of various transition aluminas formed by the dehydration of boehmite have been extensively investigated. Several studies demonstrate the close relationship between the microstructural features of boehmite and the structure and texture of the resulting transition aluminas [1,7,10–15]. The few papers [16–21] published on the kinetics of the boehmite dehydration generally give conflicting results. As pointed out by Tsuchida et al. [20], the discrepancies between them are attributable to the differences in particle size, specific surface area and crystallinity of the boehmite used for the experiments. Most of these kinetic studies assume that the dominating reaction process is a single rate-controlling process throughout all stages of the reaction. Furthermore, it is often accepted that the associated activation energy remains constant during the dehydration process. In this work, we clearly show that these assumptions are inaccurate for nanocrystalline boehmite.

The main goal of the present paper is to report a comprehensive investigation of the dehydration kinetics of nanocrystalline boehmite synthesized by hydrolysis of aluminum alkoxide. In kinetic studies, a precise knowledge of the structural and microstructural features of the involved materials is essential, therefore the first part of this paper reports the thorough characterization of both nanocrystalline boehmite and its dehydration products. Using a material with a very small crystal size is critical when dehydration affects the structure rather than the surface layer. With larger crystals the limiting step is very often the diffusion of gas through the solid and the true kinetic parameters cannot be determined. Finally, it is worth noting that, given the importance of boehmite in coatings or in catalysts manufacturing, good modeling of its dehydration kinetics would be very useful for the accurate design of industrial thermal processes.

2. Experimental

2.1. Synthesis

Three kinds of boehmite samples were synthesized according to the well-known Yoldas process [22–25], which consists of introducing aluminum tri-sec-butoxide (ASB) $Al(OC_4H_9)_3$ in an excess of distilled water (H_2O/Al = 100) under vigorous stirring at 85 °C. Stirring was maintained for 15 min. The first sample (S1) was obtained by drying the hydrolyzed slurry at 50 °C in air (no peptization). For the second sample (S2), the hydroxide precipitate was peptized by adding 0.07 mol of nitric acid per mol of alkoxide and stirring at 85 °C until a clear sol is obtained (∼24 h). For the third sample (S3), peptization was done with 0.20 mol of nitric acid per mol of alkoxide.

2.2. Powder X-ray diffraction (PXRD)

The crystal structure was investigated by powder X-ray diffraction. Data were collected on a Seifert 3003TT $\theta-\theta$ diffractometer in Bragg–Brentano geometry, using filtered Cu Kα radiation and a graphite secondary-beam monochromator. Diffraction intensities were measured by scanning from 5 to 90° (2θ) with a step size of 0.02° (2θ).

Whole powder pattern fitting (WPPF) was done by the le Bail method using the software *PowderCell* developed by Nolze and Kraus [26]. The reflection profiles were modeled by pseudo-Voigt functions. The peak positions were constrained by lattice parameters. The variation of the peak FWHMs (full-width at half-maximum) across the pattern were calculated from the classical Caglioti [27] formula.

2.3. Specific surface area and density

The specific surface areas were computed from the N_2 adsorption isotherms (recorded at 77 K with a Micromeritics ASAP 2010), using the Brunauer–Emmett–Teller (BET) method.

Skeletal densities of powder were determined using a gas pycnometer (Micromeritics AccuPyc 1330) and working with helium. Each experimental value results from the average of 10 successive measurements on the same sample.

2.4. Electron microscopy

Transmission electron microscopy (TEM) analyses were done on a JEOL 2010. A small amount of sample powder was put in ethanol and dispersed with ultrasound during 1 min. Then the carbon-coated grid was dipped in the suspension and allowed to dry at room temperature.

2.5. Thermal analysis

Simultaneous thermogravimetric (TG) and differential thermal (DT) analyses were carried out on a SETARAM TG-DTA 92 thermobalance using 20 mg of sample; α-alumina was used as reference.

Kinetics studies were performed with a special apparatus built around a CAHN D200 electrobalance. The balance can operate in vacuum and detect a mass change of 10^{-6} g. Generally, these experiments were done either under Ar or under a gas mixture containing 20% O_2 in Ar. The concentration of water in these gases was less than 50 ppm. A vacuum purge of atmospheric air was done before starting the experiments. This operation induces a systematic mass loss because, under vacuum, the samples start to lose water from room temperature.

2.6. Computer simulations of reactions

The computer simulations of the chemical kinetic reactions involved in the supposed reaction mechanism have been done using the classical deterministic model based on the numerical integration of a set of differential equations through time. The differential equations are the rate laws of each reaction step. The algorithm is a predictor-corrector algorithm (based on Heun's method [28]) which automatically adjusts the step size of the integration. Iterative refinement of the parameters (frequency factors, activation energies and reaction orders) was done by a non-linear least-squares method based on the simplex algorithm [28] to optimize a fit to the experimental data.

Moreover, to check the validity of the results given by the numerical integration procedure, we have also used the IBM Chemical Kinetics Simulator (CKS) program [29]. Rather than finding a solution which describes the state of the system at all points in time, this software uses a stochastic method where changes in a system are modeled by randomly selecting among probability-weighted reaction steps [30].

3. Results and discussion

3.1. Characterization of boehmite samples

TEM micrographs of the boehmite samples (Fig. 1) reveal the very small size of the crystallites. Nanocrystals of less than 10 nm can be seen, which have a strong tendency to organize themselves to build polycrystalline fibers, sheet or slabs. The main difference between the samples seems to be the ability of crystallites to undergo auto-organization. S1 gives bidimensional objects (sheets) often folded. S3 essentially contains almost monodimensional particles (fibers). S2 presents an intermediate behavior.

The X-ray diffraction patterns of the three samples are reported in Fig. 2. Except for the first reflection they appear to be very similar. The broad diffraction lines reveal that the crystallites are very small. Moreover, in the same pattern, the peak widths are also different, the first reflection being the widest. The structural elements in boehmite crystals consist of double chains of AlO_6 octahedra giving double molecules [1,31].

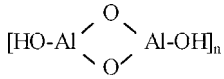

These chains are parallel, forming layers with the OH groups outside. The double chains are linked by hydrogen bonds between hydroxyl ions in neighboring planes. Boehmite crystals exhibit perfect cleavage perpendicular to the general direction of the hydrogen bonding [3].

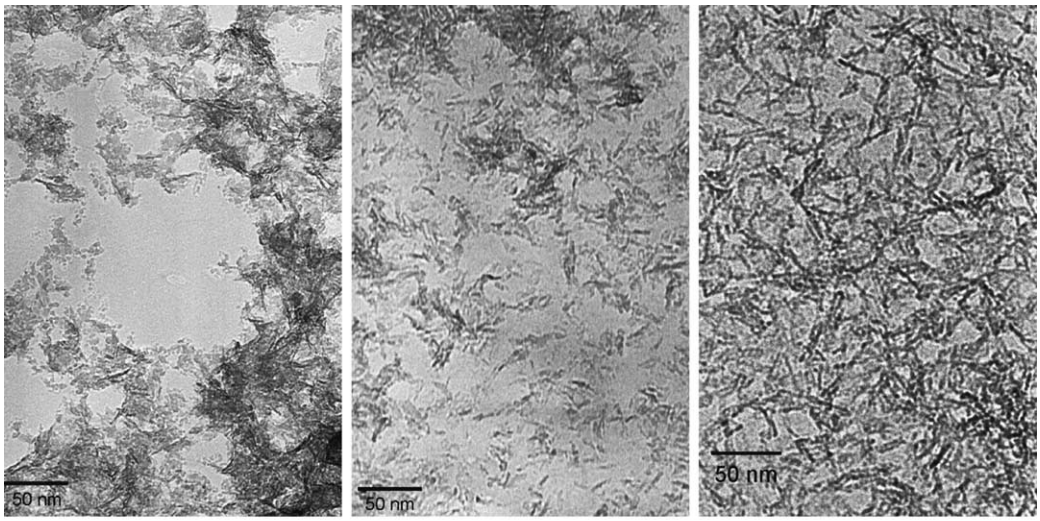

Fig. 1. TEM micrographs of the boehmite samples.

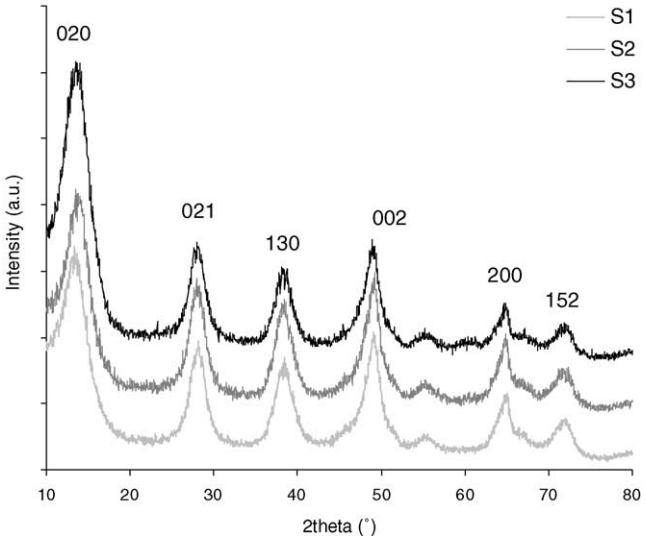

Fig. 2. X-ray diffraction patterns of boehmite samples (Cu Kα radiation). Orthorhombic unit cell, space group number 63, *Cmcm*.

This structure corresponds to an orthorhombic unit cell. The diffraction peaks have been indexed using the space group *Cmcm*. Whole pattern fitting of the experimental diagrams of Fig. 2 gives an acceptable agreement with the boehmite structure (Fig. 3) provided that the first line (0 2 0) was excluded because it presents too large a shift toward small angles from its calculated position (see Table 1). This shift of the (0 2 0) line, observed for microcrystalline boehmite, has been the subject of much controversy in the past. It has been attributed to interlayer water [31,32], or to a smaller attractive force between layers due to water absorption at the periphery of layers [33]. More recent works [5–7] have demonstrated that the (0 2 0) peak shift is essentially due to a particle-size effect like the one observed for clays [34].

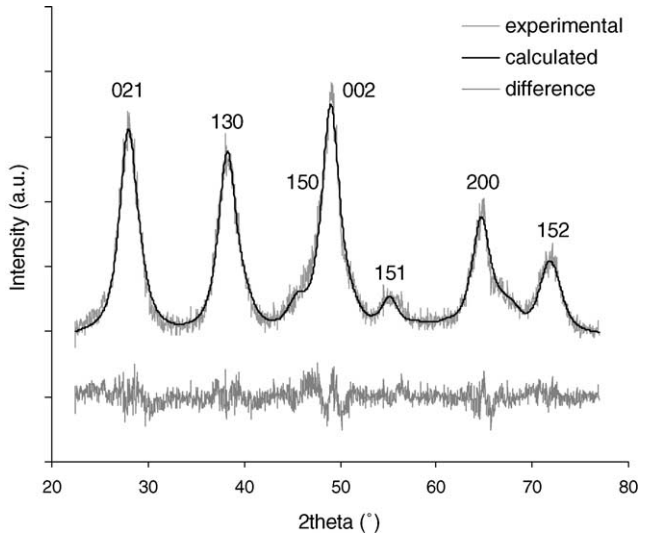

Fig. 3. Whole powder pattern fitting (le Bail method) of the experimental pattern recorded with the sample S1. Orthorhombic unit cell, space group number 63, *Cmcm*.

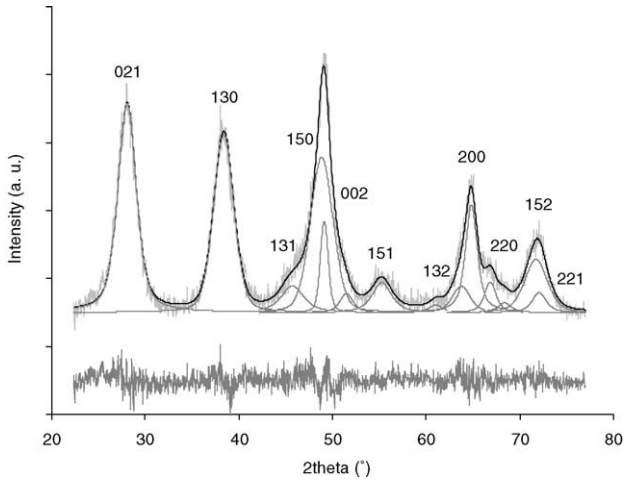

Fig. 4. Pattern decomposition of the experimental pattern recorded with the sample S1. Each diffraction profile has been modeled using a separated set of parameters (intensity, FWHM, Lorentzian fraction of pseudo-Voigt function). Orthorhombic unit cell, space group *Cmcm*.

Whole pattern fitting agreement with the experimental pattern is not very good for two groups of lines, at about 50 and 65° (2θ) (Fig. 3). This is because the crystallite shapes are anisotropic. If the refinement is done using a separate set of parameters–peak intensity, FWHM, Lorentzian fraction of pseudo-Voigt function, for modeling each diffraction profile (peak positions being fixed), the agreement between experimental and modeled patterns improves (Fig. 4). The widths of the 0 0 2 and 2 0 0 reflections are smaller than the others because the crystallite dimensions along the *a*- and *c*-axes are larger than along the *b*-axis, which means that crystallites have a platelet shape. Such a shape has often been reported for microcrystalline boehmite and can be related to the fact that the cleavage plane is perpendicular to the *b*-axis. The refined FWHM of the 2 0 0, 0 2 0 and 0 0 2 lines can be used to estimate, by Scherrer's equation, the average crystallite size along the *a*-, *b*- and c-axis. The instrumental broadening contribution was evaluated by using α-alumina (S1 calcinated at 1400 °C for 2 h) as standard. The results, reported in Table 1, show that crystallites are rectangular plates averaging 8 by 9 nm and 2–3 nm in thickness. This size is in good agreement with the size of the elementary particles observed by TEM.

The marked enhancement in intensity of the 0 2 0 diffraction line indicates that a large fraction of the crystallites have their *b*-axis oriented in a direction close to normal to the sample holder plane. This texture is due to the plate shape of the crystallites and has already been reported [35–37] for microcrystalline boehmite.

The values of the cell parameters corresponding to the best fit are very similar for the three samples (Table 1) and they are close to the parameters reported in literature (a = 2.868 Å; b = 12.214 Å; c = 3.694 Å) for crystallized boehmite [38]. From the cell parameters, we have also calculated the cell volume and the crystal density (Table 1).

Table 1
Characteristics of boehmite samples

	S1 not peptized	S2 peptized with 0.07 mol HNO_3/Al	S3 peptized with 0.21 mol HNO_3/Al
2θ shift (°) for 0 2 0 line	1.05 ± 0.01	0.74 ± 0.01	0.86 ± 0.01
a (nm)	0.287 ± 0.0005	0.287 ± 0.0005	0.287 ± 0.0005
b (nm)	1.222 ± 0.001	1.219 ± 0.001	1.223 ± 0.001
c (nm)	0.371 ± 0.0005	0.371 ± 0.0005	0.371 ± 0.0005
Cell volume/nm^3	0.130 ± 0.0005	0.130 ± 0.0005	0.130 ± 0.0005
Crystal density/g cm^{-3}	3.063 ± 0.012	3.071 ± 0.012	3.059 ± 0.012
D200 (nm)	6.3 ± 0.2	7.3 ± 0.2	8.5 ± 0.2
D020 (nm)	2.8 ± 0.1	2.9 ± 0.1	2.5 ± 0.1
D002 (nm)	9.0 ± 0.3	9.0 ± 0.3	8.9 ± 0.3
Specific surface area/m^{2}g^{-1}	352 ± 0.4	341 ± 1.5	256 ± 0.5
L.O.I. (wt.%)	30.5 ± 0.5	28.5 ± 0.5	32.0 ± 0.5
Al_2O_3 (%)	69.5 ± 0.5	71.5 ± 0.5	68.0 ± 0.5
AlOOH (%)	81.8 ± 0.5	84.1 ± 0.5	80.0 ± 0.5
Formula	$AlO(OH)\cdot 0.74H_2O$	$AlO(OH)\cdot 0.63H_2O$	$AlO(OH)\cdot 0.83H_2O$
Experimental density (g cm^{-3})	2.355 ± 0.0004	2.478 ± 0.0005	2.378 ± 0.0007
Calculated density (g cm^{-3})	∼2.2	∼2.3	∼2.2

The specific surface area, measured after outgassing 15 h at 100 °C, are close to 350 m^2/g for S1 and S2, but only 260 m^2/g for S3. Yoldas reported that the specific surface area is affected by the amount of acid used for peptization [22]. He found that a critical amount of acid was needed to peptize the hydroxide to a clear sol (the acid concentration is about 0.07 mol per mol of Al). Increasing this amount increases the repulsive force between colloidal particles and enlarges the gelling volume which has a negative influence on various properties of the oxide resulting from this gel.

By measuring the loss on ignition (LOI), which is the mass loss after calcination at high temperature (2 h at 1200 °C), the total amount of water contained in the samples is obtained because they are transformed into α-alumina which is pure Al_2O_3. The expected mass loss for the formation of anhydrous boehmite AlOOH, according to

$$2\,AlOOH \rightarrow H_2O + Al_2O_3 \quad (1)$$

would be 15%. Our samples contain about twice this amount (Table 1). Such values are not uncommon for very small boehmite crystallites [12,14,15,31,39].

As stated above, two models have been reported to explain the water excess in boehmite; surface water adsorbed on the particles [33] and inter-layer water in the crystal structure of boehmite [31,32]. The second hypothesis was proposed to account for the shift of the 0 2 0 line towards small angles but we have seen that this shift has been explained by a particle-size effect [5,6]. Now it is admitted that the excess of water in boehmite is simply adsorbed on the crystallite surface. A recent DFT study of the surface properties of boehmite [40] has shown that the surface energy strongly depends on the crystalline planes. The basal (0 1 0) surface, which forms about 50% of the total surface, is unreactive. Water is only physisorbed on it, whereas on the (1 0 0) and (0 0 1) surfaces, water is chemisorbed, mainly dissociatively.

From the dimensions of crystallites, an estimation of the amount of adsorbed water (physi- or chemi-sorbed) which forms a monolayer on the surface can be done [15,33]. The maximum adsorption capability for water molecules is obtained by expanding the coordination number of surface aluminum to six and of surface oxygen atoms to four (oxide or hydroxide). The number of adsorption sites for water molecules on a platelet crystallite (8 nm × 2.5 nm × 9 nm), worked out following the same model as Nguefack et al. [15], is given in Table 2. Adsorption on all the sites leads to the stoichiometry $AlOOH\cdot 0.5H_2O$. Experimentally we have between 0.63 and 0.83 H_2O in excess according to the samples (Table 1), which means that there is multilayer adsorption.

The water excess can also explain the strong discrepancy between experimental densities measured with a helium pycnometer and the densities calculated from lattice parameters (Table 1). The crystal density, calculated from the lattice parameters, is:

$$d_{\text{crystal}} = \frac{m_{\text{crystal}}}{V_{\text{crystal}}} \quad (2)$$

Similarly the experimental density d_{exp} is:

$$d_{\text{exp}} = \frac{m_{H_2O} + m_{\text{crystal}}}{V_{H_2O} + V_{\text{crystal}}} \quad (3)$$

For 1 g of sample, $m_{H_2O} + m_{\text{crystal}} = 1$ and $V_{H_2O} = m_{H_2O} = 1 - \text{AlOOH}/100$, which gives:

$$d_{\text{calc}} = \left(\frac{\%\text{AlOOH}/100}{d_{\text{crystal}}} + \left(1 - \frac{\%\text{AlOOH}}{100}\right)\right)^{-1} \quad (4)$$

The results, reported in Table 1, demonstrate that, although the calculated densities are slightly lower than the experimental values (which could mean that the real volume taken by water is less than 1 cm^3/g), the agreement is rather good.

3.2. Thermal decomposition of nanocrystalline boehmite

Typical TG–DTG–DTA curves are reported in Fig. 5a. The dehydration appears to occur in three main steps. The first

Table 2
Determination of the number of adsorption sites for water molecules for a platelet crystallite 8 × 2.5 × 9 nm (the same model as [15] has been used)

Direction	*a*	*b*	*c*
Crystal size (nm)	8	2.5	9
Cell parameters (nm)	0.287	1.22	0.37
Number of cells	25	2	25
Faces	(1 0 0)	(0 1 0)	(0 0 1)
Surface of face (nm^2)	45	133	35
Cell number (on 2 faces)	2 × 2 × 25	2 × 25 × 25	2 × 2 × 25
Atoms (cell)	2 Al_V + 2 O_{III} + 2 HO_{III}	1 HO_{III}	2 Al_{IV} + 2 O_{III} + 2 HO_{III}
Adsorption sites	600	1250	800
Molecule H_2O/nm^2	13.3	9.4	22.8
Formula	$AlO(OH)\cdot 0.12H_2O$	$AlO(OH)\cdot 0.25H_2O$	$AlO(OH)\cdot 0.1H_2O$

gives a sharp symmetrical endotherm and finishes at 200 °C. It accounts for 5–9% of the mass loss. The second step gives a broad unsymmetrical endotherm and ends before 500 °C. It represents the major part of the mass loss, about 20–25%. The last step gives no thermal event but appears as a continuous mass loss and seems to stop at about 900 °C. It only corresponds to about 3% of the mass loss. The DTG and DTA profiles seem more-or-less the same, though the shape of the second peak is different and its maximum is shifted towards higher temperatures. This discrepancy between the DTG and DTA curves, which indicates that the change in enthalpy is not directly proportional to the rate of mass loss, is generally encountered in complex reactions.

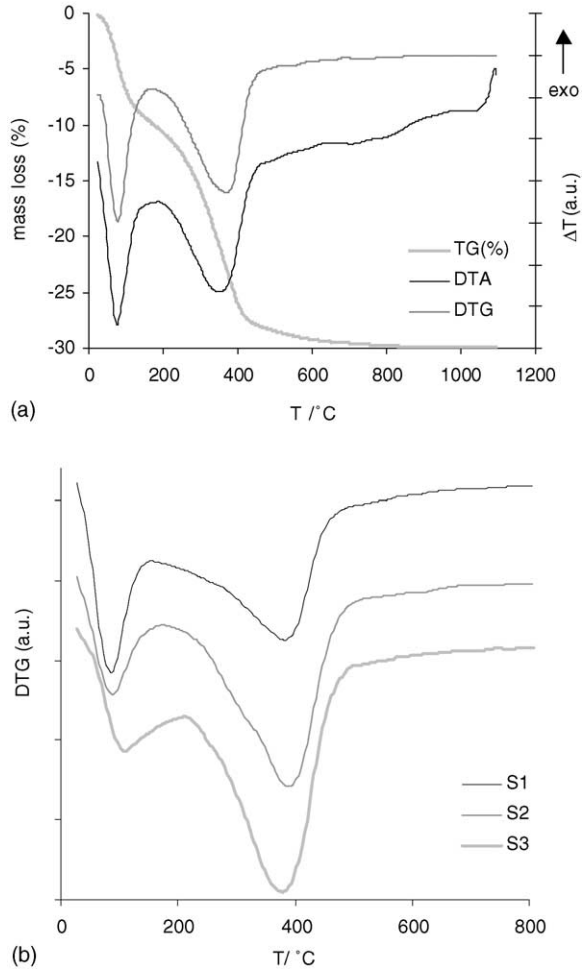

Fig. 5. a. TG–DTA curves recorded with sample S2 (mass = 20 mg, air flow = 1.5 l/h, heating rate = 120 °C/h) b. Comparison of the DTG curves for the different samples (mass = 30 mg, Ar flow = 1.5 l/h, heating rate = 150 °C/h).

The shape of the DTG curve strongly depends on the experimental conditions, such as sample mass, static or dynamic atmosphere, heating rate,... Fig. 5b illustrates that in the temperature range 20–800 °C, our samples give rather different shapes of DTG profiles.

These kind of curves have often been reported in literature [12,14,15,41]. The first step has been attributed to the desorption of physically adsorbed water, the second step to the conversion of boehmite into γ-alumina, and the last step to the elimination of residual hydroxyls. The exotherm, which appears at the very end of DTA curve, corresponds to the transformation into α-alumina. The shape of these curves has been found to be closely related to the crystal size of boehmite [12,14]. The first peak is not observed for crystals larger than 50 nm. The second peak becomes sharper as the crystal size increases and is shifted towards higher temperatures [14]. In some papers [12,15,41], to explain the asymmetrical profile of the second peak, an additional step is considered, attributed to the removal of chemisorbed water before the conversion into transition alumina.

For a given sample, the change of specific surface area, as well as the mass loss induced by heating under vacuum, have been followed. Because this mass loss essentially results from the loss of water, to help the interpretation of the experimental data, as well as the comparison between samples, it is more convenient to convert the sample mass into n_{H_2O}, where n_{H_2O} represents the number of water molecules in the sample per Al_2O_3 formula. Thus for anhydrous boehmite, AlOOH, $n_{H_2O} = 1$ while $n_{H_2O} = 0$ for $\alpha{-}Al_2O_3$. For example, in the case of a sample which had an initial mass m_i and a current mass m after being heated

$$n_{H_2O} = \frac{n_{H_2O}}{n_{Al_2O_3}} = \frac{m - m_{Al_2O_3}}{M_{H_2O}} \frac{M_{Al_2O_3}}{m_{Al_2O_3}}$$

$$\text{with} \quad m_{Al_2O_3} = m_i \frac{100 - LOI}{100} \tag{5}$$

Table 3
Effect of temperature on specific surface area

Sample	Outgassed in	T(°C)	n_{H_2O}	SBET (m^2g^{-1})
S1	Vacuum	50	1.45 ± 0.02	339 ± 0.3
S1	Vacuum	100	1.32 ± 0.02	352 ± 0.3
S1	Vacuum	150	1.16 ± 0.01	361 ± 0.3
S1	Vacuum	200	0.97 ± 0.01	377 ± 0.4
S1	Vacuum	250	0.76 ± 0.01	395 ± 0.4
S1	Vacuum	300	0.46 ± 0.01	417 ± 0.6
S1	Vacuum	325	0.32 ± 0.01	426 ± 0.7
S1	Vacuum	355	0.19 ± 0.01	433 ± 0.8
S1	Vacuum	390	0.13 ± 0.01	433 ± 0.9
S1	Vacuum	455	0.09 ± 0.01	430 ± 0.9
S1	Vacuum	465	0.08 ± 0.01	428 ± 0.9
S2	Vacuum	100	1.56 ± 0.02	341 ± 1.5
S2	Vacuum	250	1.16 ± 0.01	383 ± 1.3
S2	Vacuum	270	0.97 ± 0.01	395 ± 1.3
S2	Vacuum	300	0.79 ± 0.01	412 ± 1.1
S2	Vacuum	350	0.22 ± 0.01	456 ± 2.5
S2	Vacuum	450		468 ± 2.5
S2	Air	350		441 ± 1.3
S2	Air	400		404 ± 1.3
S2	Air	350		437 ± 1.2
S2	Air	500		339 ± 2.9
S2	Air	500		333 ± 2.9
S2	Air	700		237 ± 1.4
S2	Air	800		171 ± 0.5
S3	Vacuum	50	1.72 ± 0.03	229 ± 0.4
S3	Vacuum	100	1.58 ± 0.03	256 ± 0.5
S3	Vacuum	150	1.41 ± 0.02	282 ± 0.6
S3	Vacuum	200	1.27 ± 0.02	297 ± 0.7
S3	Vacuum	250	0.97 ± 0.02	327 ± 0.7
S3	Vacuum	265	0.78 ± 0.01	345 ± 0.7
S3	Vacuum	285	0.67 ± 0.01	354 ± 0.7
S3	Vacuum	305	0.54 ± 0.01	365 ± 0.7
S3	Vacuum	320	0.38 ± 0.01	378 ± 0.7
S3	Vacuum	350	0.23 ± 0.01	388 ± 0.8
S3	Vacuum	390	0.12 ± 0.01	386 ± 1.3
S3	Vacuum	440	0.08 ± 0.01	382 ± 1.6

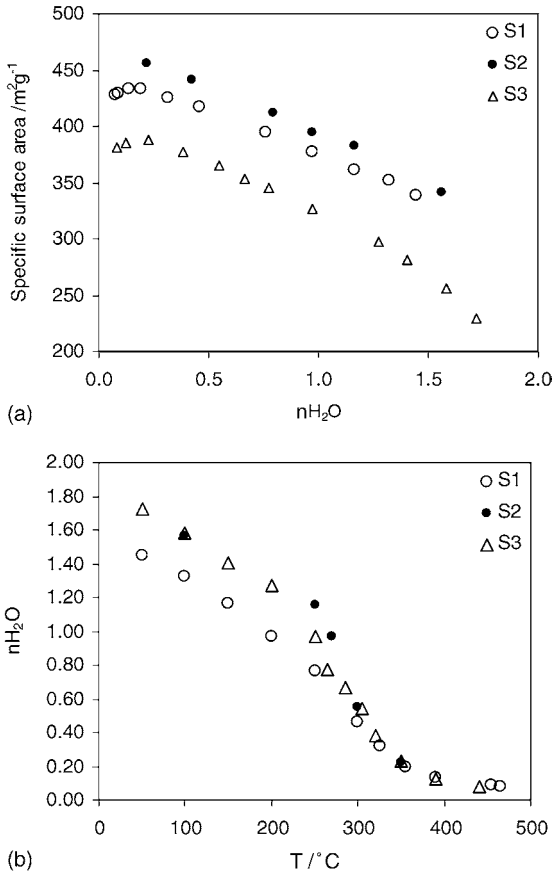

Fig. 6. a. Effect of water content on the specific surface area. For each analysis the sample was heated under vacuum (10^{-2} Pa) at the selected temperature for 18 h. To avoid a cluttered diagram, the absolute errors have not been reported, they are given in Table 3. b. Effect of temperature on the water content. For each analysis the sample was heated under vacuum (10^{-2} Pa) at the selected temperature for 18 h.

where LOI represents the loss on ignition and M_{H_2O} and $M_{Al_2O_3}$ are the molar masses of water and Al_2O_3, respectively.

For each surface analysis, the sample was heated under vacuum (10^{-2} Pa) at the selected temperature for 18 h. The results are reported in Table 3 and Fig. 6. Fig. 6a shows the dependence of BET area on n_{H_2O}, whereas Fig. 6b gives the dependence of n_{H_2O} on the temperature. The same trends can be observed for the three samples, but, for the same water content, the specific surface area differs significantly according to the sample and the difference remains for the whole range of n_{H_2O}. Fig. 6b shows that, when temperature increases, there is a linear decrease of n_{H_2O} down to $n_{H_2O} = 1$ which corresponds to AlOOH. This zone corresponds to the loss of adsorbed (physisorbed and chemisorbed) water. Water is more strongly bonded in S3 than in S1 or S2, because S3 must be heated 100 °C above S2 to reach the same value of n_{H_2O}. Below $n_{H_2O} = 1$, the conversion of boehmite into transition alumina begins and there is a steep decrease of n_{H_2O}. In this zone the plots of the three samples merge into the same curve. Values of $n_{H_2O} < 1$ were attained from 200 °C for S1. Thus, under secondary vacuum, the transformation of nanocrystallized boehmite into transition alumina can begin from 200 °C

For $n_{H_2O} > 0.2 - 0.15$ the specific surface area increases steadily along with the water loss (Fig. 6a). Because the specific surface area is the surface to mass ratio, this means that the surface area remains constant, that is the loss of water does not create any additional porosity. Actually it has been shown by Lippens [31] that the magnitude of the internal surface area formed by dehydration on heating strongly depends on the particle size of boehmite: the smaller the crystals, the smaller the increase of the surface area. This is because the dehydration is topotatic. If crystallite size of hydroxides is large (small specific surface area), when water is expelled, space will be created in the particle, which so becomes porous because the external volume of particles does not change very much [10,20,42]. But in the case of nanocrystalline boehmite, the crystallites size is so small that a large number of them contain only a few unit cell along b axis so that the collapse of the layered structure during the expelling of the water leads to the particle shrinkage but does not create significant inter-

nal porosity. The same kind of behavior has also be observed in other topotatic dehydrations like those of α-FeOOH [43] or γ-FeOOH [44]. The larger the particle size of the starting hydroxide, the larger the surface area of the iron oxide obtained.

The transformation of nanocrystalline boehmite into transition alumina starts to decrease the surface area only at the very end of the conversion, when n_{H_2O} becomes less than 0.15. This zone corresponds to the last step observed in thermal analysis.

The surface, calculated from the mean crystallite dimensions, assuming that every crystallite is a rectangular plate, is given by the formula:

$$S_{calc} = \frac{2(uv + vw + wu)}{duvw} \quad (6)$$

where d is the crystal density and u, v, w are the dimensions of the crystal. Taking $d = 3.06$, $u = 8$, $v = 2.5$ and $w = 10$ nm (cf. Table 1) gives $S_{calc} \approx 410\ m^2/g$. This value is in a rather good agreement with experimental surfaces area which confirms the absence of significant internal porosity.

Fig. 7 reports the changes in BET area with temperature for the sample S2. When the samples were heated under vacuum (filled symbols), the surface increased up to 400 °C. But when the calcination was done at atmospheric pressure (open symbols), the surface decreased from 350 °C. Hence dehydration under vacuum allows the maximum surface area to be obtained. Above 350 °C, the surface steadily decreased (about 60 m^2 per 100 °C).

In order to follow the crystal structure transformations of nanocrystalline boehmite that occur upon heating, X-ray diffraction patterns were recorded, at room temperature, on samples heated under air for 2 h at specific constant temperatures. The patterns obtained with the S3 sample are reported in Fig. 8. The crystal structure of boehmite remains up to 350 °C. For higher temperatures, the intensities of the boehmite lines decrease, while new reflections characteristic of the spinel-type structure of transition alumina progressively appear. No

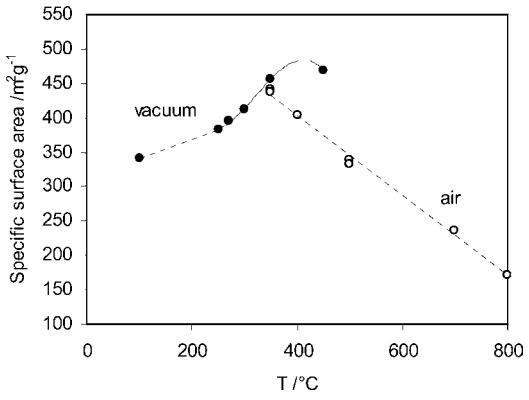

Fig. 7. Effect of temperature on the specific surface area. The filled symbols correspond to samples heated under vacuum, while open symbols correspond to samples calcined in air at atmospheric pressure.

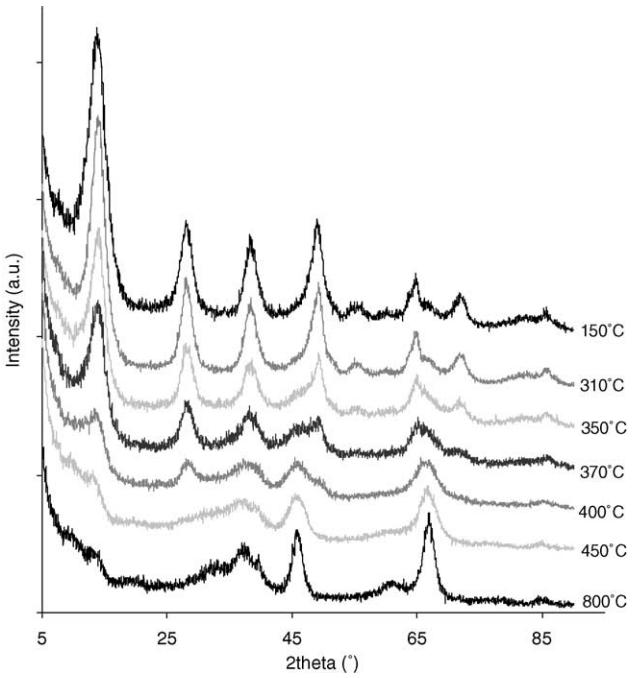

Fig. 8. Gradual change of the X-ray diffraction patterns during the thermally stimulated conversion of boehmite (S3 sample) to transition alumina; (Cu Kα radiation).

intermediate compound is formed at any temperature, and the conversion of boehmite into alumina is gradual. Up to 450 °C, the 0 2 0 line of boehmite can be detected, thus the whole temperature range of decomposition exceeds 100 °C.

From 450 °C, whole pattern fitting with a model based on cubic spinel-type structure (space group number 227, $Fd\bar{3}m$) gives good agreement, if a separate set of parameters is used for each reflection (Fig. 9). As stated above, both γ-alumina and η-alumina have a spinel-type structure, generally reported as tetragonally deformed. However γ-alumina exhibits a more pronounced tetragonal distortion than η-alumina. Although the intensity of (1 1 1) reflection appears to be rather low, there is almost no tetragonal deformation, which suggests that these patterns could correspond to η-alumina. Lippens [31] reported that the thermal decomposition of well-crystallized boehmite produced γ-alumina, while pseudoboehmite gave the η form. Even though η-alumina appears at relatively low temperatures, no sign of the formation of δ- or θ-alumina was detected up to 800 °C. The cell parameters are similar over the whole temperature range (a = 0.792 ± 0.001 nm).

3.3. Kinetic analysis of the transformation of boehmite into transition alumina

As seen above, the thermal decomposition of nanocrystalline boehmite to transition alumina is a complex process involving four consecutive stages. Using the same formulation as Tsukada et al. [12], the reaction mechanism can be

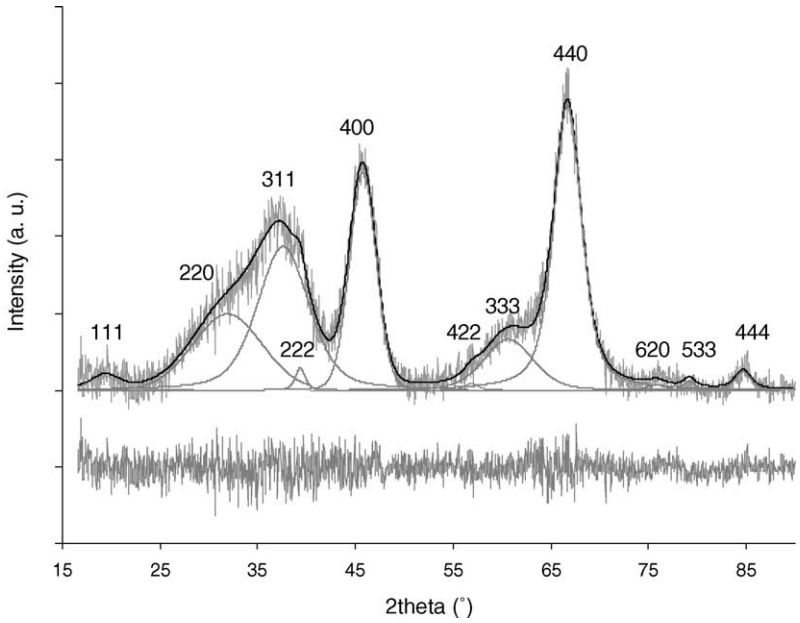

Fig. 9. Pattern decomposition of the experimental pattern recorded with the sample S3 heated in air at 450 °C. Unit cell cubic, space group number 227, $Fd\bar{3}m$.

written:

desorption of physisorbed water :

$$(\mathrm{AlOOH})_2 \cdot (m+n)\mathrm{H_2O} \rightarrow n\mathrm{H_2O} + (\mathrm{AlOOH})_2 \cdot m\mathrm{H_2O} \quad (7)$$

desorption of chemisorbed water :

$$(\mathrm{AlOOH})_2 m\mathrm{H_2O} \rightarrow m\mathrm{H_2O} + 2\mathrm{AlOOH} \quad (8)$$

conversion into transition alumina :

$$2\mathrm{AlOOH} \rightarrow (2-\nu)/2\mathrm{H_2O} + \mathrm{Al_2O_{3-\nu/2}(OH)_\nu} \quad (9)$$

dehydration of transition alumina :

$$\mathrm{Al_2O_{3-\nu/2}(OH)_\nu} \rightarrow \nu/2\mathrm{H_2O} + \mathrm{Al_2O_3} \quad (10)$$

where m and n are, respectively, the number of physisorbed and chimisorbed water molecules on the surface of boehmite, and ν is the number of residual hydroxyl groups remaining in the transition alumina.

The goal of this study was to determine the kinetics parameters for each step, i.e., the activation energy E_a, the pre-exponential factor A_o, and the reaction order, as well as the m, n and ν values. We can reasonably assume that the kinetics parameters of each step do not change during the reaction course because: (i) the reaction proceeds through an almost constant surface area, except for the last step; (ii) the process only involves short-range rearrangements of atoms in the crystal structure; that is, the transformations are topotactic; (iii) the particle are very small so that the size effects are minimized.

In order to evaluate the variation of the activation energy with the extent of the reaction, an isoconversional method has been used. Isoconversional methods are based on the principle that the reaction rate at a constant extent of conversion is only a function of temperature [45]. In practice, several experiments should be carried out under the same conditions (atmosphere, pressure, flow rate, sample mass,...) only changing the heating rate (β). Then, for a given fraction transformed (α), a plot of $\ln(\beta)$ versus $1/T$ should give a straight line. For a constant heating rate and using the Doyle approximation [46], the slope is about $-1.052\ E_a/R$. However, because we obtained rather low activation energies, we used the correction for the Doyle approximation introduced by Flynn [47].

As above, the curves mass = $f(t)$ have been converted into $n_{H_2O} = f(t)$ where n_{H_2O} stands for the number of water molecule per Al_2O_3 formula. The reaction coordinate, or fraction transformed (α), was determined by:

$$\alpha(t) = \frac{n_0 - n_t}{n_0 - n_f} \quad (11)$$

where n_0 is the value of n_{H_2O} at the beginning of the process, n_t the value at the time t and n_f at the end of the process. The results obtained using values of β in the range 30–600 °C h^{-1} are reported in Fig. 10 and clearly confirm the complexity of the reaction. E_a is approximately 40 kJ/mol for the first step ($0 < \alpha < 0.2$, loss of weakly adsorbed water). It increases to 130 kJ/mol for the second step ($0.2 < \alpha < 0.6$, loss of chemisorbed water) and increases further to 160 kJ/mol for the third step ($0.6 < \alpha < 0.9$, conversion of boehmite into transition alumina). Finally E_a decreases to 90 kJ/mol for the last step ($0.9 < \alpha < 1.0$, dehydration of transition alumina). Standard deviations were very large for α below 0.4. This reveals that, in this range, E_a depends on the heating rate.

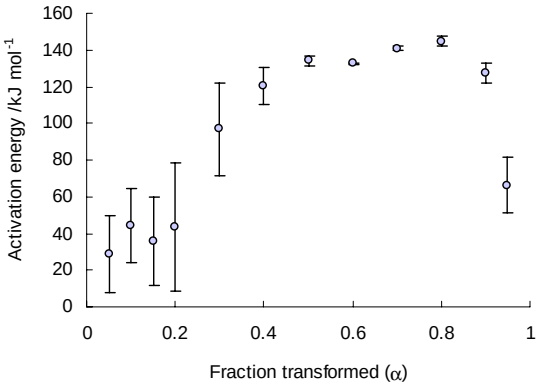

Fig. 10. Activation energies determined by an isoconversional method (Flynn [47]).

It has been demonstrated [48] that E_a depends on the heating rate in reversible reactions and, as we will see below, at low temperatures the reverse reaction (hydration) cannot be neglected.

Our experimental device was not well designed for isothermal studies because the reaction rate becomes rapid before the furnace has reached the target temperature. However, in order to study the first step separately, some experiments were done in the low temperature region (up to 100 °C). After the short heating ramp, the sample was maintained at a constant temperature until there was no significant change of the sample mass with time. The final equilibrium value of n_f depended on temperature. This behavior has already been reported in kinetic studies of boehmite [18]. This means that, in this temperature range, the sample reached a stable water content for each temperature. On the other hand, several studies have shown that increasing the water vapor pressure causes the rate constant to decrease but has little effect on the activation energy [17,20]. The straightforward interpretation is that thermodynamic equilibrium between direct (dehydration) and reverse (hydration) reaction was reached. Because the gas purge contained a very low amount of water (<50 ppm), the rate constant of hydration should be considerably larger than that for dehydration.

We have simulated this equilibrium using a set of two equations:

$$\text{dehydration } P \rightarrow H_2O + C \tag{12}$$

$$\text{hydration } H_2O + C \rightarrow P \tag{13}$$

where P, the compound containing physisorbed water—$(AlOOH)_2\cdot(m + n)H_2O$ in Eq. (7)—gives C which only contains chemisorbed water.

The kinetics of these reactions are described by the differential equation:

$$\frac{d[P]}{dt} = -\frac{d[C]}{dt} = k_d(T)[P] - k_h(T)[C] \tag{14}$$

where [P] and [C] are the concentrations of each species and $k_d(T)$ and $k_h(T)$ are the rate constants for dehydration and hydration, respectively. The concentration of water is not taken into account because, since we were working in a flowing atmosphere it is assumed to be constant and can be incorporated in the rate constant. Hence we have three parameters for each reaction (E_a, A_o and the initial concentration). The simulation process consists of iteratively searching for the values of the parameters which give the best fit (by a non-linear least-squares method) between the experimental data and the cumulative concentration of the H_2O species computed from numerical integration of these equations through time. The time-temperature dependence is taken from the experimental curve.

As in any non-linear least square refinement process, reasonable initial values of the fitting parameters are needed to avoid convergence to a local minimum rather than to the global minimum. For the activation energy of dehydration we have taken 45 kJ/mol which is the value found by the Flynn method. The dehydration being endothermic, the activation energy of the reverse reaction should be less than the energy of the direct step and the difference between these values is equal to the enthalpy of the reaction. We have assumed that this energy is of the same magnitude as a hydrogen bond. An average value for the hydrogen bond energy is 30 kJ/mol [49], hence the activation energy of hydration was taken as 15 kJ/mol. We have taken P = C = 0.4, as initial values for P and C, because the starting value for n_{H_2O} after outgassing at room temperature was about 1.8, which means that the sum P + C should be about 0.8. Moreover, the sum P + C was constrained to remain equal to 0.8. Initial values for A_o have been estimated by trial and error in such a way that the calculated curve was not too far from the experimental one.

The results of the simulations of some experimental tests, realized with different heating ramps and plateau temperatures, are reported in Table 4. The quality of fitting is evaluated by the goodness of fit (GoF) defined as:

$$\text{GoF} = \sqrt{\frac{\sum_i w_i(y_i(\text{exp}) - y_i(\text{calc}))^2}{(N - N_P)}} \tag{15}$$

where y_i(exp) are the experimental values, y_i(calc) the values calculated by numerical integration, w_i the weight attributed to each y_i(exp), N the number of experimental points and N_P the number of parameters.

The fit obtained for a plateau temperature of 100 °C is worse than the others because, at this temperature, the second step (loss of chemisorbed water) was beginning. In all cases the best fit was obtained for rather similar E_a values: about 50 kJ/mol for dehydration and 30 kJ/mol for hydration. The difference between these energies, that is the enthalpy of dehydration, is in the range 20–30 kJ/mol. Fig. 11 illustrates that this model, based on an equilibrium between adsorption and desorption of water, allows the shape of the experimental curves, especially the initial portion where the sample adsorbs water, to be simulated well. The values of A_o for hydration

Table 4
Simulations of the first step of the thermal dehydration of boehmite sample S2—mass, 25 mg; atmosphere, Ar

$T_{plateau}$ (°C)	70	80	90	100
β (°C h^{-1})	300	150	500	300
GoF	110	270	230	390
P	0.45 ± 0.01	0.44 ± 0.01	0.47 ± 0.01	0.45 ± 0.01
C	0.35 ± 0.01	0.36 ± 0.01	0.33 ± 0.01	0.35 ± 0.01
A_o dehydration	39500 ± 200	6860 ± 80	199000 ± 1000	81200 ± 2000
A_o hydration	13 ± 0.1	2.05 ± 0.03	3.5 ± 0.2	26 ± 1
E_a dehydration (J mol^{-1})	52600 ± 100	46200 ± 400	58200 ± 200	54600 ± 1000
E_a hydration (J mol^{-1})	31000 ± 200	24200 ± 400	27200 ± 200	33300 ± 1000
GoF	110	240	210	
A_o (s^{-1})	65700 ± 1000	10500 ± 300	415000 ± 10000	
E_a (J mol^{-1})	51700 ± 200	44250 ± 400	54600 ± 400	
Order	1.2 ± 0.05	1.5 ± 0.10	1.9 ± 0.05	

are far lower than for dehydration but, as stated above, A_o is the product of the true pre-exponential factor and the concentration of water in the gas flow. Because this concentration is very low (about 50 ppm) the true pre-exponential factor for hydration is actually larger than for dehydration.

It is clear that the same kind of equilibrium exists for the second step and indeed a computation using a model based on two successive reversible reactions (simulated by four reactions) gives a good fit with experimental data recorded for samples heated above 100 °C. However, when the whole process is considered, this increases the complexity considerably because six reactions rather than four are then involved and it would be an illusion to believe that it is possible to evaluate so many parameters with reliability.

We can reduce the complexity and return to the initial mechanism (with four reactions) if the first-order reversible reactions are simulated by only one reaction, but with an order different from one. Of course the price to pay is that the first part of the curve (initial adsorption of water at low temperature) cannot be correctly modeled. The results of the simulations, using this simplified one-reaction model, are reported at the bottom of Table 4. These computations were done on the same experimental data as above, but the first part of the curves were ignored. They gave similar GoF, except for the data of the last column for which agreement was poor. In all cases, the activation energies are slightly lower than the activation energies of dehydration.

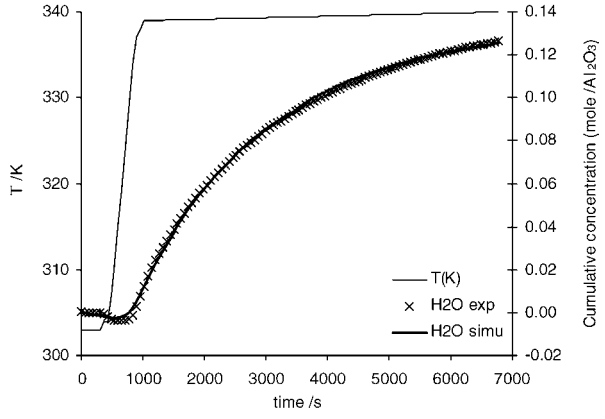

Fig. 11. Simulation of the first reaction step (loss of physisorbed water) with a model based on an equilibrium between adsorption and desorption of water. For the sake of clarity, the number of experimental points has been divided by 2. (Sample S2 under Ar flow).

The last task is the simulation of the whole process by the set of Eqs. (7)–(10). However, in this mechanism, the first three reactions are consecutive; this restriction is actually supported by no experimental evidence and, especially, nothing requires that conversion into transition alumina should only take place when boehmite has lost its adsorbed water. Hence in our simulations, we have replaced Eqs. (7) and (8) by the Eqs. (16) and (17):

$$\text{desorption of physisorbed water}: \quad P \rightarrow H_2O + B1 \quad (16)$$

$$\text{desorption of chemisorbed water}: \quad C \rightarrow H_2O + B2 \quad (17)$$

$$\text{conversion into transition alumina}: \quad 2AlOOH \rightarrow (2-\nu)/2H_2O + Al_2O_{3-\nu/2}(OH)_\nu \quad (18)$$

$$\text{dehydration of transition alumina}: \quad Al_2O_{3-\nu/2}(OH)_\nu \rightarrow \nu/2H_2O + Al_2O_3 \quad (19)$$

where, as above, P is the compound containing physisorbed water and C contains only chemisorbed water. The species B1 and B2 are not used in the following steps, thus we have three parallel reactions.

At this stage, recalling that a correct analysis uses as few adjustable parameters as possible, it should be emphasized that even if the peaks corresponding to step 2 and 3 are partly overlapping, only a set of four (at least) equations allow to obtain a correct fitting of the experimental curves. Nevertheless that does not demonstrate the uniqueness of the kinetic parameters corresponding to the best fit of a single curve. Therefore the choice of the starting values for the parameters is very important, especially the activation energy.

Initial values for activation energies were those found by the isoconversional method of Flynn. We have taken C = 0.5 as an initial value for C, and P = n_{ini} − C where n_{ini} was the starting value for n_{H_2O} after outgassing at room temperature. The sum P + C was constrained to remain equal to n_{ini}. As

Table 5
Simulations of the thermal dehydration of boehmite

Sample	S2-f	S2-g	S2-j	S2-k	S2-e	S2-r	S2-m	S2-c	S2-t	S2-b	S2-u	S1-b	S3-b
Atmosphere	Ar	Ar	Ar	Ar	Ar	Ar	20%O_2/Ar	Vacuum 100 Pa	Ar	Ar	Ar	Ar	Ar
β (°C h^{-1})	300	300	300	150	60	30	300	150	150	150	150	150	150
m (mg)	30	30	30	30	30	30	30	30	30	30	10	30	30
Initial n_{H_2O}	1.75	1.72	1.70	1.71	1.72	1.70	1.77	1.70	2.00	2.23	1.75	1.86	1.86
GoF	280	260	280	520	500	560	450	680	720	530	670	890	510
P	0.35	0.34	0.33	0.36	0.36	0.38	0.42	0.35	0.61	0.60	0.42	0.51	0.50
C	0.40	0.38	0.36	0.35	0.35	0.32	0.35	0.35	0.39	0.63	0.33	0.35	0.36
ν	1/2	1/2	1/2	1/2	1/2	1/2	1/2	1/2	1/2	1/2	1/2	1	1/2
Order step 1	2.4	2.3	2.4	2.8	2.9	3.0	2.4	2.9	2.6	2.9	2.5	1.6	3.0
Order step 2	1.0	1.0	1.0	1.0	1.0	1.0	1.1	1.4	0.9	1.7	0.9	1.2	1.0
Order step 3	1.3	1.2	1.2	1.3	1.4	2.0	1.3	1.5	1.4	1.3	1.7	2.1	1.4
Order step 4	3.0	2.8	2.7	2.8	2.9	2.8	2.9	2.6	3.0	2.9	3.0	3.0	3.0
E_a step 1 (J mol^{-1})	44	45	45	42	43	39	44	36	42	44	40	44	46
E_a step 2 (J mol^{-1})	60	60	60	60	59	60	59	51	59	62	59	54	61
E_a step 3 (J mol^{-1})	115	115	115	115	114	113	112	105	113	118	113	109	117
E_a step 4 (J mol^{-1})	63	64	63	63	65	65	65	51	63	68	63	52	68
A_o step 1 (s^{-1})	5100	4400	4500	4800	3800	1400	7700	3000	6100	5200	6200	3600	4300
A_o step 2 (s^{-1})	420	410	440	360	140	220	430	110	330	430	410	410	440
A_o step 3 (s^{-1})	194000	164000	168000	154000	107000	95900	138000	141000	147000	218000	175000	418000	328000
A_o step 4 (s^{-1})	7	7	7	5	4	17	12	4	6	7	10	9	19

For the sake of clarity, errors have not been reported and values have been rounded. Maximum relative errors are less than 5% for order, 1% for E_a and 10% for A_o.

previously, initial values for A_o have been estimated by trial and error so that the curve calculated from the initial guesses was not too far from the experimental one. Moreover, ν was not refined as the other parameters. Five simulations were done, taking successively ν = 1, 2/3, 1/2, 2/5 and 1/3.

The results of the simulations, obtained with different samples, heating ramps, and atmospheres are reported in Table 5. Though these experiments have been done under various conditions, the values of the parameters giving the best fit with experimental data are generally remarkably similar, especially the activation energies. The simulated curves follow the experimental profiles very closely as shown in Fig. 12. To check that the numerical integration procedure has given correct results, we have fed the CKS program (see experimental) with the equation of each step and the parameters of Table 5. It can be seen in Fig. 13 that the agreement is perfect. On the other hand, this figure confirms that the first three reactions are not consecutive but parallel. The loss of chemisorbed water begins although physisorbed water still remained. Similarly transition alumina appears even though boehmite still contains almost 50% of chemisorbed water. Fig. 13 also indicates that transition alumina is formed above 300 °C, which is in good agreement with our previous findings (Section 1.2).

The three first columns (S2-f, S2-g, S2-j) of the Table 5 demonstrate that three similar samples tested under the same conditions lead to very similar results. The small differences in the starting value for n_{H_2O} are due to the difficulty of achieving the same outgassing.

The E_a of step 1 is generally very close to the value found by the Flynn method. However, for the next steps, E_a is significantly lower than predicted by this method: 60 kJ/mol for the 2nd step, 110–120 kJ/mol for the third and only 60–70 kJ/mol for the fourth. It is interesting to notice that the E_a of the third step (conversion of boehmite into transition alumina) is close to the heat of chemisorption of H_2O on γ-Al_2O_3 [50]. This step could be limited by the difficulty of removing strongly chemisorbed water. The E_a of the last step is very low for a reaction occurring in the temperature range 400–500 °C, but all the attempts to increase this energy lead to worse fits. A reason for so low an activation energy could be that a diffusion process essentially limits this step. The order of the first step is generally close to 3 which indicates the reversibility of this step. Conversely, the second step is found to be approximately a first-order process, which shows a minor contribution of the reverse reaction.

The sample S2-m has been analyzed using a flowing gas mixture of 20%O_2 in Ar. Comparison with samples heated under Ar with the same heating rate (the three first columns) shows that oxygen plays no role in the dehydration process. A_0, for the step 1, was found to be larger probably because the O_2-containing mixture was drier than the Ar.

The sample S2-c has been analyzed under vacuum. We have worked under a relatively high pressure (100 Pa) because, for lower values, the TG signal was too noisy. It is clear that working under vacuum induces a shift towards lower temperatures. All the E_a values are found to be lower. The rate of the second step is also decreased. We have seen above that, under secondary vacuum, the conversion of boehmite into transition alumina begins from 200 °C. This demonstrates that the kinetics of the whole process are governed by the partial pressure of water.

The samples S2-k, S2-t and S2-b contained different amounts of adsorbed water but were otherwise analyzed under the same conditions. The initial value of n_{H_2O} seems to affect the reaction parameters only when it becomes larger

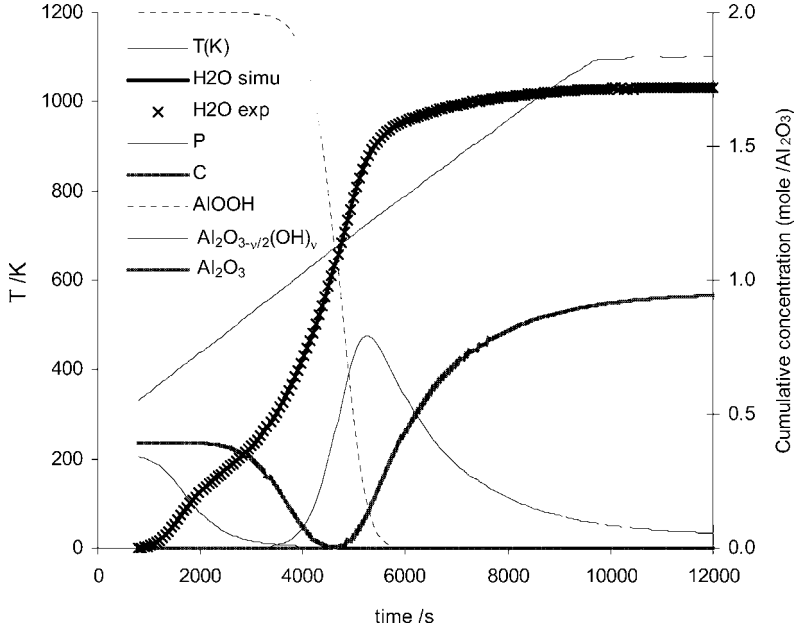

Fig. 12. Simulation of the whole reaction with a model, based on four reaction steps. For the sake of clarity, the number of experimental points has been divided by 2. (Sample S2 under Ar flow, β = 300 °C/h).

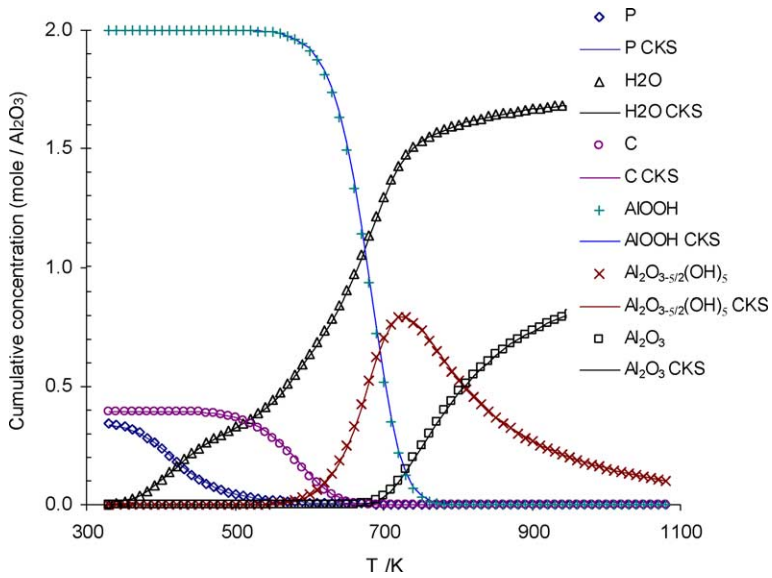

Fig. 13. Comparison between simulation of the whole reaction i) by the numerical integration of the differential equations (symbols) ii) by the stochastic method used by the IBM Chemical Kinetics Simulator (CKS) program [29] (full curves). The experimental data are the same as in Fig. 12.

than 2.0. This can be linked to the fact that, for $n_{H_2O} \approx 2.0$, the surface is fully covered. Above that value there is formation of a multilayer.

For the samples S2 and S3, the best fits were obtained for $\nu = 1/2$; but for the sample S1, the optimum was found for $\nu = 1$. These high values, for the number of residual hydroxyl groups remaining in transition alumina, can be explained by the fact that, as pointed out before, there is still a lot a chemisorbed water when transition alumina starts to form.

4. Conclusions

Hydrolysis of ASB according to the Yoldas method yields nanocrystalline boehmite with crystallites which are rectangular platelets averaging 8 by 9 nm and 2–3 nm in thickness. This nano-sized boehmite contains a large excess of water. When water is eliminated by heating under secondary vacuum, an increase in the specific surface area is observed down to a minimum water content (≈0.2 H_2O per Al_2O_3). Values up to 470 m^2/g can be reached. However, this enlargement of specific surface area is only due to the loss of water, the surface area remaining constant. Though the conversion into transition alumina can begin from 200 °C, the temperature at which the maximum surface is observed is about 350 °C. The surface steadily decreased (about 60 m^2 per 100 °C) when the sample was heated beyond this temperature. The particle morphology, the excess of water, as well as the specific surface area, depend on the amount of acid used for the peptization during the synthesis. The transition alumina has a cubic spinel-type structure with almost no tetragonal deformation. No significant change, either in the crystal structure or in the cell parameter, was detected up to 800 °C ($a = 0.792 \pm 0.001$ nm).

The kinetic simulations of the non-isothermal experiments at constant heating rates show that the thermally stimulated transformation of nanocrystalline boehmite into alumina can be modeled by a 4-reaction mechanism involving: (i) the loss of physisorbed water, (ii) the loss of chemisorbed water, (iii) the conversion of boehmite into transition alumina, (iv) the dehydration of transition alumina (loss of residual hydroxyl groups).

The activation energies of each step are found to be very similar for experiments done under various conditions (heating rate, atmosphere, kind of sample,. . .). Values found are 40–45 kJ/mol for the first reaction, 50–60 kJ/mol for the second, 105–115 kJ/mol for the third and 50–70 kJ/mol for the last. The first reaction is actually an equilibrium because, at low temperature, the hydration rate is larger than the dehydration rate. Formation of transition alumina occurs although boehmite still contains chemisorbed water, which could explain the large number of residual hydroxyl groups. The surprisingly low activation energy found for the last reaction probably reveals that the dehydration of transition alumina is essentially limited by a diffusion process.

Acknowledgements

The authors would like to thank Mr. Lucien Datas (CIRIMAT) for the TEM work. This research was done in the frame of the MINIREF (ENK6-CT-2001-00515) project supported by the E.C.

References

[1] B.C. Lippens, J.H. De Boer, Acta Crystallogr. (1964) 17.
[2] R.L. Zhou Rong-Sheng, Snyder, Acta Crystallogr. Sect. B: Struc. Sci. B47 (1991) 617–630.

[3] K. Wefers, G.M. Bell, Oxides and Hydroxides of Aluminium Alcoa Technical Paper, No. 19, Alcoa Laboratories, 1987.
[4] R.B. Bagwell, G.L. Messing, Critical factors in the production of sol–gel derived porous alumina, in: D.-M. Liu (Ed.), Porous Ceramic Materials, Key Eng. Mater. 115 (1996) 45–64.
[5] R.T. Tettenhorst, D.A. Hofmann, Clays Clay Miner. 28 (1980) 373–380.
[6] R.T. Tettenhorst, C.E. Corbato, Clays Clay Miner. 36 (1988) 181–183.
[7] M. Bellotto, B. Rebours, P. Euzen, Proceedings of the Fifth European Powder Diffraction Conference 1997, Material Science Forum, 1998, pp. 572–577.
[8] X. Bokhimi, J.A. Toledo-Antonio, M.L. Guzman-Castillo, F. Hernandez-Beltran, J. Solid State Chem. 159 (2001) 32–40.
[9] A.E. Gobichon, B. Rebours, P. Euzen, Mater. Sci. Forum 378–381 (2001) 523–528.
[10] S.J. Wilson, J. Solid State Chem. 30 (1979) 247–255.
[11] C. Simon, R. Bredesen, H. Grondal, A.G. Hustoft, E. Tangstad, J. Mater. Sci. 30 (1995) 5554–5560.
[12] T. Tsukada, H. Segawa, A. Yasumori, K. Okada, J. Mater. Chem. 9 (1999) 549–553.
[13] M.L. Guzman-Castillo, X. Bokhimi, A. Toledo-Antonio, J. Salmones-Blasquez, F. Hernandez-Beltran, J. Phys. Chem., B 105 (2001) 2099–2106.
[14] X. Bokhimi, J.A. Toledo-Antonio, M.L. Guzman-Castillo, B. Mar-Mar, F. Hernandez-Beltran, J. Navarrete, J. Solid State Chem. 161 (2001) 319–326.
[15] M. Nguefack, A.F. Popa, S. Rossignol, C. Kappenstein, Phys. Chem. Chem. Phys. 19 (2003) 4279–4289.
[16] C. Eyraud, R. Goton, J. Chim. Phys. 51 (1954) 430–433.
[17] W.D. Callister Jr., I.B. Cutler, R.S. Gordon, J. Am. Ceram. Soc. 49 (1966) 419–422.
[18] L. Abrams, M.J.D. Low, Ind. Eng. Chem. Prod. Res. 8 (1969) 38–48.
[19] E. Buzagh-Gere, J. Simon, S. Gal, Fresenius Z. Anal. Chem. 264 (1973) 392–396.
[20] T. Tsuchida, R. Furuich, T. Ishii, Thermochim. Acta 39 (1980) 103–115.
[21] M.H. Stacey, Langmuir 3 (1987) 681–686.
[22] B.E. Yoldas, J. Mater. Sci. 10 (1975) 1856–1860.
[23] B.E. Yoldas, Am. Ceram. Soc. Bull. 54 (1975) 286–288.
[24] B.E. Yoldas, Am. Ceram. Soc. Bull. 54 (1975) 289–290.
[25] B.E. Yoldas, US Patent, 3,941,719 (1976).
[26] W. Kraus, G. Nolze, J. Appl. Crystallogr. 29, 1996. 301-303 (PowderCell for Windows, Federal Institute for Materials Research and Testing (BAM), Berlin, Germany http://users.omskreg.ru/∼kolosov/bam/a_v/v_1/powder/e_cell.htm).
[27] G. Caglioti, A. Paoletti, F.P. Ricci, Nucl. Instr. 3 (1958) 223–228.
[28] A.F. Carley, P.H. Morgan, Computational methods in the chemical sciences, Ellis Horwood, 1989 (for Heun's method, p. 168, for Simplex algorithm, p. 269).
[29] IBM Chemical Kinetics Simulator (CKS) program https://www.almaden.ibm.com/st/computational_science/ck/msim/?cks.
[30] F.A. Houle, W.D. Hinsberg, Surf. Sci. (1995) 338.
[31] B.C. Lippens, Structure and Texture of Aluminas, Thesis, Delft (1961).
[32] D. Papee, R. Tertian, R. Biais, Bull. Soc. Chim. Fr. (1958) 1301–1310.
[33] B.R. Baker, R.M. Pearson, J. Catal. 33 (1974) 265–278.
[34] R.C. Reynolds Jr., Acta Crystallogr. A24 (1968) 319–320.
[35] W.O. Milligan, H.B. Weiser, J. Phys. Colloid Chem. 55 (1951) 490–496.
[36] J. Campaniello, P. Berthet, F. D'Yvoire, A. Revcolevschi, J. Mater. Res. 10 (2) (1995) 297–301.
[37] A.F. Popa, S. Rossignol, C. Kappenstein, J. Non-Cryst. Solids 306 (2002) 169–174.
[38] G.G. Christoph, C.E. Corbato, D.A. Hofmann, R.T. Tettenhorst, Clays Clay Miner. 27 (1979) 81–86.
[39] C.T. Wang Shan-Li, D.L. Johnston, J.L. Bish, S.L. Hem White, J. Colloid Interface Sci. 260 (2003) 26–35.
[40] P. Raybaud, M. Digne, R. Iftimie, W. Wellens, P. Euzen, H. Toulhoat, J. Catal. 201 (2001) 236–246.
[41] J.A. Wang, X. Bokhimi, A. Morales, O. Novaro, T. Lopez, R. Gomez, J. Phys. Chem., B 103 (1999) 299–303.
[42] J. Rouquerol, F. Rouquerol, M. Ganteaume, J. Catal. 36 (1975) 99–110.
[43] L.A. Perez-Maqueda, J.M. Criado, C. Real, J. Subrt, J. Bohacek, J. Mater. Chem. 9 (1999) 1839–1845.
[44] G.S. Chopra, C. Real, M.D. Alcala, L.A. Perez-Maqueda, J. Subrt, J.M. Criado, Chem. Mater. 11 (1999) 1128–1137.
[45] S. Vyazovkin, C.A. Wight, Int. Rev. Phys. Chem. 17 (1998) 407–433.
[46] C.D. Doyle, J. Polym. Appl. Sci. VI 24 (1962) 639–642.
[47] J.H. Flynn, J. Ther. Anal. 27 (1983) 95–102.
[48] S. Vyazovkin, W. Linert, Int. J. Chem. Kinet. 27 (1995) 73–84.
[49] L.J. Michot, F. Villieras, M. François, I. Bihannic, M. Pelletier, J.-M. Cases, C. R. Geosci. 334 (2002) 611–631.
[50] J.M. McHale, A. Auroux, A.J. Perrota, A. Navrotsky, Science 277 (1997) 788–791.